

# Journal of Materials Chemistry A

Accepted Manuscript



This is an *Accepted Manuscript*, which has been through the Royal Society of Chemistry peer review process and has been accepted for publication.

*Accepted Manuscripts* are published online shortly after acceptance, before technical editing, formatting and proof reading. Using this free service, authors can make their results available to the community, in citable form, before we publish the edited article. We will replace this *Accepted Manuscript* with the edited and formatted *Advance Article* as soon as it is available.

You can find more information about *Accepted Manuscripts* in the [Information for Authors](#).

Please note that technical editing may introduce minor changes to the text and/or graphics, which may alter content. The journal's standard [Terms & Conditions](#) and the [Ethical guidelines](#) still apply. In no event shall the Royal Society of Chemistry be held responsible for any errors or omissions in this *Accepted Manuscript* or any consequences arising from the use of any information it contains.

## ARTICLE

# Na<sub>3</sub>V<sub>2</sub>(PO<sub>4</sub>)<sub>3</sub>@C core-shell nanocomposites for rechargeable sodium-ion batteries

Cite this: DOI: 10.1039/x0xx00000x

Received 00th January 2012,  
Accepted 00th January 2012

DOI: 10.1039/x0xx00000x

www.rsc.org/

10 Wenchao Duan, Zhiqiang Zhu, Hao Li, Zhe Hu, Kai Zhang, Fangyi Cheng and Jun Chen\*

Na<sub>3</sub>V<sub>2</sub>(PO<sub>4</sub>)<sub>3</sub> (NVP) is an attractive cathode material for sodium ion batteries due to its high theoretical energy density and stable three-dimensional (3D) NASICON structure. In this paper, NVP@C core-shell nanocomposite has been synthesized through a hydrothermal assisted sol-gel method. Ascorbic acid and polyethylene glycol 400 (PEG-400) were synergistically used to control the particle growth and provide the surface coating of conductive carbon. The as-prepared nanocomposite was composed of a nanosized Na<sub>3</sub>V<sub>2</sub>(PO<sub>4</sub>)<sub>3</sub> core with typical size of ~40 nm and a uniformly amorphous carbon shell with the thickness of a few nanometers. The electrode performance of NVP@C core-shell nanocomposite as cathode for sodium ion batteries is investigated and compared with bare NVP and NVP/C. Among the samples examined, the NVP@C nanocomposite showed the best cycle life and rate capability. It rendered an initial capacity of 104.3 mAh g<sup>-1</sup> at 0.5C and 94.9 mAh g<sup>-1</sup> at 5C with a remarkable capacity retention of 96.1% after 700 cycles. Moreover, a full cell using the as-prepared nanocomposite as both the cathode and anode active material has been successfully built, showing a reversible capacity of 90.9 mAh g<sup>-1</sup> at 2C with an output voltage of about 1.7V and a specific energy density of about 154.5Wh kg<sup>-1</sup>. The enhanced electrode performance is attributed to the combination of particle downsizing and carbon coating that can favor the migration of both electrons and ions.

## Introduction

Lithium ion batteries (LIBs) have displayed a large proportion in the global market of rechargeable batteries.<sup>1-3</sup> However, there is still much concern whether the viable lithium resource on earth could afford the increasing large-scale applications.<sup>4,5</sup> As sodium is one of the most abundant elements and exhibits similar chemical properties to lithium, sodium ion batteries (NIBs) are promising alternatives in future battery technologies.<sup>6-9</sup> However, the storage and cycling abilities of NIBs are generally inferior to their lithium counterparts due to the bigger ionic radius of Na<sup>+</sup> and the larger volume change upon Na/Na<sup>+</sup> removal or insertion.<sup>10</sup> Therefore, desirable electrode materials for NIBs should adopt robust and flexible crystal structures that can accommodate large sodium ions. In this context, many electrode materials such as layered transition sodium oxides Na<sub>x</sub>MO<sub>2+y</sub> (M = Mn, Co, V etc.), olivine NaMPO<sub>4</sub> (M = Fe, Mn, etc.) and sodium super ionic conductor (NASICON) Na<sub>x</sub>M<sub>2</sub>(PO<sub>4</sub>)<sub>3</sub> (M = V, Ti, etc.) have been investigated.<sup>9,11-17</sup> Among various cathode materials for NIBs, Na<sub>3</sub>V<sub>2</sub>(PO<sub>4</sub>)<sub>3</sub> (NVP) with NASICON structure has received extensive interest owing to its advantages of high Na<sup>+</sup> ion conductivity, small volume change upon Na<sup>+</sup> intercalation/deintercalation, moderate potential plateau (3.4 V), high theoretical energy density (400 Wh/kg), and high thermal stability.<sup>18-20</sup>

Nevertheless, NVP still suffers from intrinsic low electric conductivity, which limits the practical rate capability and cycling ability. In the case of the other polyanionic compounds, carbon coating and particle downsizing have been often attempted to improve the performance.<sup>21-23</sup> The coating of nanosized NVP particle with a thin carbon layer to form a NVP@C core-shell nanostructure is particularly favorable because of simultaneously reduced diffusion length for Na<sup>+</sup> intercalation and enhanced electron conduction. However, the preparation of NVP@C nanocomposite is not an easy task. The formation of NVP phase with large anionic framework generally involves a high-temperature calcination process, in which NVP tends to grow and aggregate into large grains.<sup>16,18,20</sup> Additionally, it is challenging to achieve the homogeneity of both particle size and surface carbon coating.

Recently, we have developed a hydrothermal-assisted sol-gel method for the synthesis of uniform nanosized Li<sub>3</sub>V<sub>2</sub>(PO<sub>4</sub>)<sub>3</sub>@C core-shell nanocomposites for LIBs.<sup>24</sup> The key of the synthesis is the hydrothermal pretreatment of reactants, in which partially-carbonized species are evenly coated on the phosphate precursors to restrict particle enlargement during the followed calcination process. Herein, we extend the synthetic concept for NVP@C nanocomposites. The electrochemical properties of NVP@C core-shell nanostructures in NIBs are investigated and

compared with bare NVP and NVP/C particles. The NVP@C core-shell nanocomposites exhibit remarkable electrode performance such as prolonged cycling life, enhanced rate capability, and low polarization. Furthermore, two redox couples of  $V^{4+}/V^{3+}$  and  $V^{3+}/V^{2+}$  endow NVP with two different voltage plateaus at 3.4 V and 1.6 V, respectively. This shows that NVP is a suitable candidate either as the cathode or as the anode. Thus, we construct rechargeable sodium-ion full cells by applying the as-prepared NVP@C nanocomposite as the initial active materials of both the cathode and anode. The battery can work well with an output voltage of  $\sim 1.7$  V and realize a specific energy density of  $154.5 \text{ Wh kg}^{-1}$ . A preliminary test shows that a cycle life exceeding 50 cycles with an initial capacity of  $90.9 \text{ mAh g}^{-1}$  and a capacity retention of 81.4% at 2C was obtained.

## Experimental

### Synthesis

Three kinds of NVP materials including NVP@C nanocomposite (nano NVP@C), NVP/C composite (NVP/C) and bare NVP (NVP) were synthesized in this work. The nano NVP@C was obtained by a hydrothermal assisted sol-gel approach. In a typical synthesis, 4 mmol  $V_2O_5$ , 12 mmol  $NH_4H_2PO_4$  and 6 mmol  $Na_2CO_3$  were added to 70 mL of distilled water and magnetically stirred at room temperature. Then, 6 mmol ascorbic acid and 6 mL polyethylene glycol 400 (PEG-400) were added to form a blue suspension, which was stirred for 30 min before being transferred to a 100 mL Teflon-lined autoclave. The sealed autoclave was kept at 180 °C for 40 h, and then naturally cooled to room temperature. The resulting brown mixture was ultrasonically treated for 90 min to make a uniform dispersion and then heated on a hot plate at 95 °C with stirring to evaporate water. The obtained brown sol was dried in 120 °C overnight. This precursor was thoroughly ground and preheated at 350 °C for 4 h. The preheated sample was ground to powders and finally calcined at 750 °C for 6 h in flowing Ar atmosphere. For comparison, NVP/C composite was prepared via a similar method to that of nano NVP@C but without the hydrothermal process. NVP was synthesized using similar procedure to that for NVP/C composite except using  $H_2C_2O_4$  as the reductant with the molar ratio of  $V_2O_5:H_2C_2O_4 = 1:3$ .

### Material characterization

The as-synthesized samples were characterized by powder X-ray diffraction (XRD, Rigaku MiniFlex600, Cu  $K\alpha$  radiation). XRD patterns were refined by the Rietveld refinement program GSAS.<sup>25</sup> The morphologies and microstructures of the samples were observed by scanning electron microscopy (SEM, JEOL JSM7500F) and transmission electron microscopy (TEM, Philips Tecnai F20). The specific surface area and pore size distribution were measured by Brunauer-Emmett-Teller (BET) nitrogen

adsorption-desorption measurement (Japan, BELSORP-Mini). The carbon layer was analyzed by Raman spectroscopy (DXR, ThermoFisher Scientific, 532 nm excitation) and elemental analyzer (German, VarioEL).

### Electrochemical investigation

Electrochemical measurements were carried out using CR2032 coin cells. The working electrodes were made by blending 80 wt% of the active material, 10 wt% of the KS6 graphite, and 10 wt% of the polyvinylidene difluoride (PVDF) binder in N-methyl-2-pyrrolidone. The obtained slurry was pasted onto aluminum foil and dried at 110 °C for 10 h in vacuum to evaporate N-methyl-2-pyrrolidone. Sodium metal was used as the anode for half cells. The full cell was constructed using nano NVP@C as both cathode and anode with the capacity limitation of the cathode. The weight ratio of the cathode and anode was about 3:5. The electrolyte was propylene carbonate (PC) containing 1M  $NaClO_4$ . Cells were assembled in an argon-filled glove box. The assembled cells were cycled at different charge-discharge rates on a Land CT2001A cell testing system. The cyclic voltammograms (CV) performed on a Parstat 263A potentiostat/galvanostat workstation. Impedance measurements were conducted by using a 2273 potentiostat/galvanostat workstation with an amplitude of 5 mV over the frequency range from 100 kHz to 10 mHz. Electrochemical impedance spectroscopy (EIS) was collected at the conditions of 50% depth-of-discharge,  $\sim 3.4$  V potential, 5th cycle and 1C rate. All the electrochemical measurements were tested at 298 K.

## Results and Discussion

The  $Na_3V_2(PO_4)_3$  adopts the NASICON structure with R-3c space-group, as shown in Fig. 1a. Each octahedron corner of  $VO_6$  shares with three  $PO_4$  tetrahedrons. One  $Na^+$  occupies the M1(6b) site and the other two are located in M2(18e) site of the interstitial sites.<sup>9,18,26</sup> The  $VO_6$  octahedrons and  $PO_4$  tetrahedrons together constitute a highly covalent three-dimensional framework. The channel between two  $PO_4$  tetrahedrons combined with the voids between a  $PO_4$  tetrahedron and a  $VO_6$  octahedron as well as a curved pathway are possible for sodium ion diffusion, eliciting the favourable 3D transport character.<sup>27</sup> Powder X-ray diffraction (XRD) patterns of the obtained samples are shown in Fig. S1. All reflections can be indexed to pure  $Na_3V_2(PO_4)_3$  phase as reported in previous literature.<sup>15,18</sup> Fig. 1b shows the XRD pattern of nano NVP@C with refined Rietveld analysis. The calculated pattern matches well with the experimental profile with a relatively low  $R_{wp}$  (8.17%) and  $R_p$  (6.21%). This indicates that the purity of the phase is high. The cell parameters are calculated to be  $a = 8.72 \text{ \AA}$ ,  $c = 21.81 \text{ \AA}$ ,  $\alpha = 90^\circ$ , and  $\gamma = 120^\circ$ .

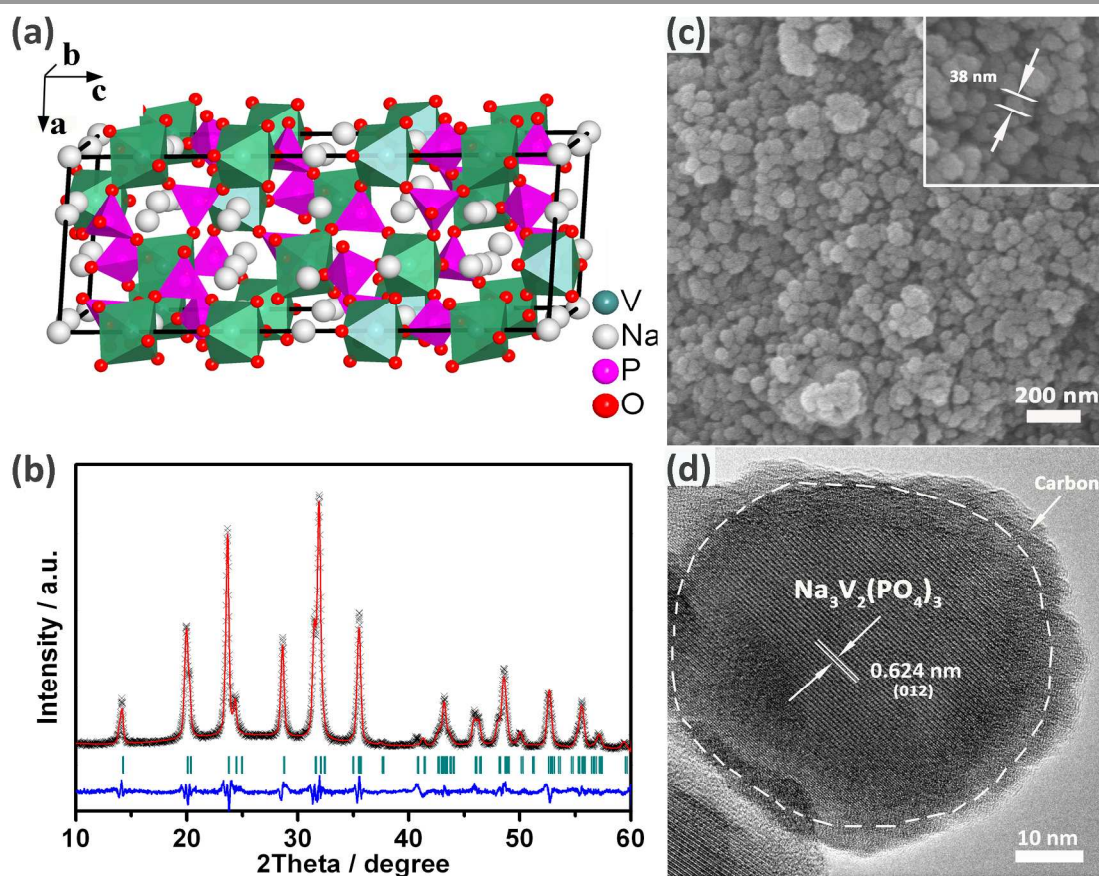


Fig. 1 (a) Crystal structure of NASICON  $\text{Na}_3\text{V}_2(\text{PO}_4)_3$ . (b) Rietveld refined XRD pattern, (c) SEM image, and (d) HRTEM image of the obtained nano NVP@C.

Fig. 1c shows the SEM image of nano NVP@C, which displays a uniform distribution of the nanoparticles. The average diameter of the nanoparticles is around 40 nm. Additionally, the nanoparticles seem to arrange themselves to form inter-particle voids, resulting in a porous structure that is favorable toward increasing the contact between the electrode and the electrolyte. The HRTEM image of nano NVP@C (Fig. 1d) clearly reveals that an amorphous carbon shell is coated on the surface of crystallized nano  $\text{Na}_3\text{V}_2(\text{PO}_4)_3$  with the thickness of a few nanometers, demonstrating the successful formation of nano core-shell structure. The clear lattice fringes with d-spacing of 0.624 nm correspond to (012) plane of NASICON  $\text{Na}_3\text{V}_2(\text{PO}_4)_3$ , indicating highly crystalline characteristics. Meanwhile, the proposed nano core-shell structure has been further supported by more TEM images as shown in Fig. S2. The formation mechanism of nanostructured grains has been systematically discussed in our previous report.<sup>24</sup> Briefly, the hydrothermal treatment makes ascorbic acid partly carbonize and then uniformly coat on the precursor, which has been confirmed by TEM and Raman measurements of the

precursors (Fig. S3). During the high-temperature calcinations, the partly carbonized organics and PEG-400 were completely transformed to a well coated carbon layer. This significantly prevents particle agglomeration and thus generates uniform nanosized grains. On the contrary, if only ascorbic acid or PEG-400 was used, the products displayed irregular and agglomerated morphology with larger sizes (Fig. S4). This indicates that the combination of ascorbic acid and PEG-400 plays an essential role in the formation of nano NVP@C. In comparison, NVP/C composite and bare NVP also showed pure NASICON structure (Fig. S1). Without using hydrothermal treatment or ascorbic acid and PEG-400, the particle sizes become irregular and larger (Fig. S5). Therefore, the hydrothermal-assisted sol-gel method is useful to the synthesis of nanosized  $\text{Na}_3\text{V}_2(\text{PO}_4)_3$ @C composite.

The carbon contents of nano NVP@C, NVP/C, and NVP obtained by elemental analysis are 12.5 wt%, 11.8 wt%, and 0 wt%, respectively. The Raman spectrum was also recorded for nano NVP@C (Fig. 2). Two obvious bands were observed at  $1350\text{ cm}^{-1}$  (D band) and  $1600\text{ cm}^{-1}$  (G band)

related to typical Raman features of carbon.<sup>28</sup> The peak intensity ratio of D to G band ( $I_D/I_G$ ) is 0.96, showing a high degree of graphitization with high conductivity.<sup>29,30</sup> The two broad peaks of each sample can be deconvoluted into four peaks (labeled peaks 1–4) using a Gaussian numerical simulation.<sup>31</sup> As we have reported before, the fitted  $A_{sp3}/A_{sp2}$  value provides useful information on the nature of carbon.<sup>24</sup> For nano NVP@C, this value is 0.31, suggesting a high content of  $sp^2$  type carbon. Therefore, the results indicate that the coated carbon layer favors the enhanced electrical conduction.

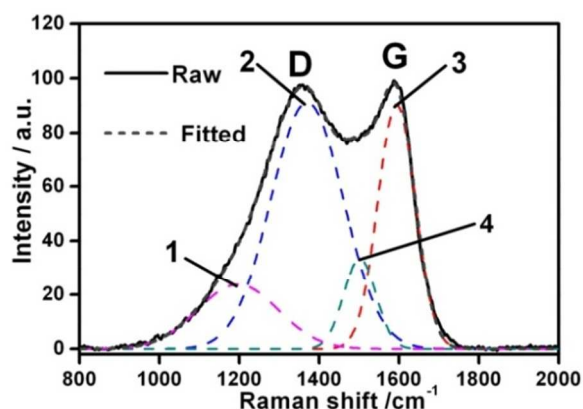


Fig. 2 Raman spectrogram of nano NVP@C electrode.

Fig. 3 shows the nitrogen adsorption/desorption isotherm and pore size distribution curves of nano NVP@C. For NVP/C and NVP, the tested results are presented in Fig. S6. Among the three samples, nano NVP@C has the largest surface area of  $109.6 \text{ m}^2 \text{ g}^{-1}$ , which is much larger than that of NVP/C ( $30.9 \text{ m}^2 \text{ g}^{-1}$ ) and NVP ( $4.97 \text{ m}^2 \text{ g}^{-1}$ ). The impressive high surface area of nano NVP@C is mainly attributed to the existence of pores generated by the accumulation of nanosized particles, just as observed in the SEM image (Fig. 1c). The pore size distribution curve determined using the BJH method shows peaks around 10–40 nm, verifying the mesoporous character. This high surface area and nanoporous structure favor the penetration of electrolyte and promote the interfacial contact,<sup>32–36</sup> thus leading to better solid state diffusion kinetics of sodium intercalation.

Further investigations of the electrochemical performance for the prepared samples were carried out. Fig. 4a displays the typical charge and discharge profiles of the three samples with a potential range of 2.5–3.8 V at a rate of 0.5C. All curves have the charge and discharge flat plateaus around 3.4 V which are consistent with the previous reports.<sup>18,19</sup> The

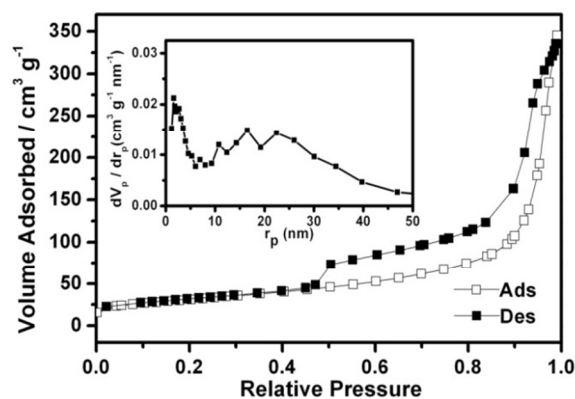
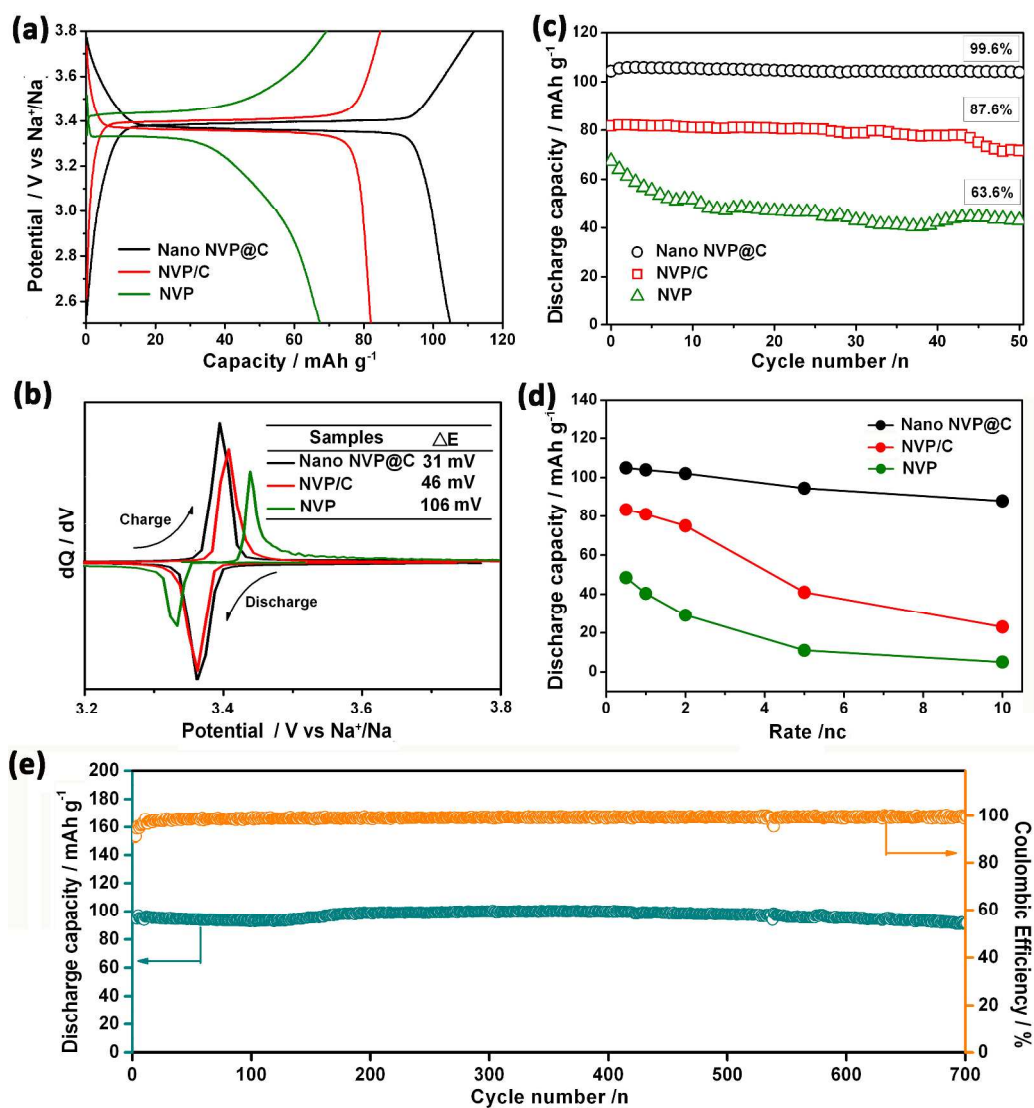


Fig. 3 Nitrogen adsorption and desorption isotherm of nano NVP@C. (inset: Pore size distribution curves)

capacity of nano NVP@C reached  $104.3 \text{ mAh g}^{-1}$ , which is about 88.4% of its theoretical value ( $118 \text{ mAh g}^{-1}$ ). Such a high capacity indicates that the small nanosized particles could realize the high utilization of the active materials. On the contrary, the discharge capacities of NVP/C and NVP are only  $81.7$  and  $67.4 \text{ mAh g}^{-1}$ , respectively. Fig. 4b shows the corresponding  $dQ/dV$  plots. A couple of the oxidation and reduction peaks which are attributed to the  $V^{4+}/V^{3+}$  redox couples can be clearly seen for the three samples. This is similar to the CV profiles (Fig. S7). Notably, nano NVP@C exhibits the most highly symmetrical sharp peaks. The values of potential polarizations ( $\Delta E$ ) for nano NVP@C is only 31 mV (insert of Fig. 4b), which is not only relative lower among the reported results for  $\text{Na}_3\text{V}_2(\text{PO}_4)_3$ ,<sup>15,19</sup> but also comparable to that of  $\text{LiFePO}_4$  in LIBs.<sup>37</sup> Such a small  $\Delta E$  fully justifies the lower electrode polarization and easier migration of Na ions, which should be benefited from the nanosized particles with a conductive coating. The cyclic performance of the three samples at 0.5C is compared in Fig. 4c. After charge and discharge for 50 cycles, the capacity retention of nano NVP@C, NVP/C, and NVP is 99.6%, 87.6%, and 63.6%, respectively. Fig. 4d shows the rate capability of the three samples at 0.5C to 10C. Obviously, nano NVP@C has the highest capacities at all tested rates. Even at 10C, it could offer a capacity of  $88 \text{ mAh g}^{-1}$ , corresponding to 83.9% of the capacity obtained at 0.5C. The minute capacities gap between different rates may facilitate the applications of the battery system at high rate. The long cycling stability at high rate of nano NVP@C was further studied at 5C rate. In Fig. 4e, the initial discharge capacity was  $94.9 \text{ mAh g}^{-1}$ , and 96.1% of this value was still retained after 700 cycles. In addition, the coulombic efficiency can reach up to approximately 100% in the overall battery operation, demonstrating a prominent high-rate cycling performance of nano NVP@C. This can be traced to its unique nano core-



**Fig. 4** Electrochemical properties of nano NVP@C, NVP/C, and NVP. (a) Typical charge and discharge profiles, (b) corresponding dQ/dV plots, (c) cyclic performance of different electrodes at 0.5C, (d) comparison of the rate capability of the three sample, and (e) coulombic efficiency and specific reversible capacity versus cycle number for nano NVP@C at 5C rate for 700 cycles.

5 shell structure with porous character.

Electrochemical impedance spectroscopy (EIS) was performed to investigate the kinetics of the electrode process. The Nyquist plots and equivalent circuit of the three samples were presented in Fig. 5a. All curves contain a semicircle in the high frequency and a straight line in the low frequency, suggesting that the electrochemical process is controlled by both charge transfer and sodium ion diffusion.<sup>23,38</sup> The diameter of the semicircle in the high frequency region on the  $Z'$  axis is approximately equal to charge transfer impedance ( $R_{ct}$ ).<sup>39,40</sup> Obviously, nano NVP@C exhibits the

lowest  $R_{ct}$ , signifying the best sodium ion intercalation kinetics. The diffusion coefficients of the three samples were calculated.<sup>39</sup> The linear plot is associated with the diffusion of  $\text{Na}^+$  ions in the cathode material. The sodium ion diffusion coefficient can be calculated using the following equation<sup>39</sup>:

$$D = \frac{R^2 T^2}{2 A^2 n^4 F^4 C^2 \sigma^2} \quad (1)$$

Where R is the gas constant, T is the absolute temperature, A is the surface area of the electrode, n is the number of

electrons per molecule during oxidization,  $F$  is the Faraday constant,  $C$  is the concentration of sodium ion, and  $\sigma$  is the Warburg factor related to  $Z'$ :

$$Z' = R_D + R_L + \sigma \omega^{-1/2} \quad (2)$$

Fig. 5b displays the relationship between  $Z'$  and reciprocal square root of frequency ( $\omega^{-1/2}$ ) in the low frequency region. The calculated diffusion coefficient of sodium ion ( $D_{\text{Na}}$ ) of nano NVP@C, NVP/C and NVP are  $2.4 \times 10^{-13}$ ,  $6.94 \times 10^{-14}$  and  $1.84 \times 10^{-15}$   $\text{cm}^2 \text{s}^{-1}$ , respectively. This demonstrates that the combined action of carbon coating and nanostructure could significantly promote electron conduction and sodium ion diffusion, thus giving high-rate capability.

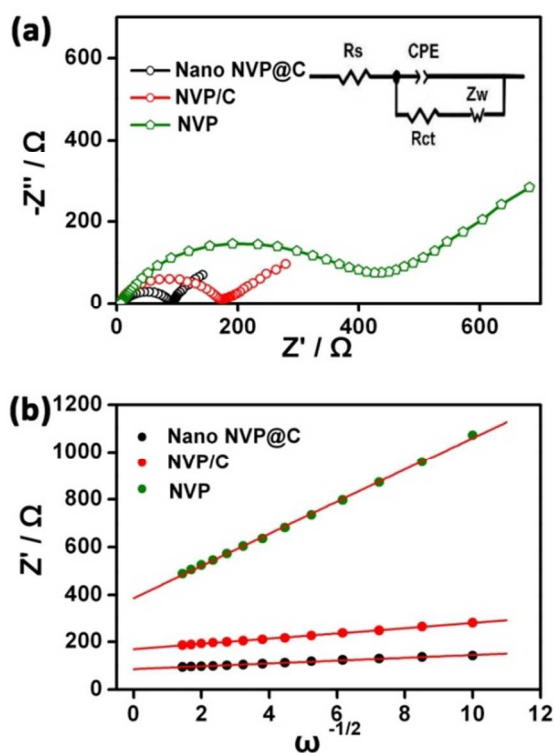


Fig. 5 (a) The Nyquist plots and equivalent circuit of nano NVP@C, NVP/C and NVP; (b) The relationship between  $Z'$  and  $\omega^{-1/2}$  in the low frequency region.

To further understand the remarkable electrode performance of nano NVP@C, the electrode tested after 50 cycles at 1C rate was investigated by XRD and TEM. As shown in Fig. 6, intensive diffraction peaks in XRD patterns and clear lattice fringes corresponding to the  $\text{Na}_3\text{V}_2(\text{PO}_4)_3$  phase in HRTEM image are well maintained after cycling test. Meanwhile,  $\text{Na}_3\text{V}_2(\text{PO}_4)_3$  core with carbon shell could be clearly seen from the HRTEM image (Fig 6a), suggesting that nano core-shell structure of the electrode could be essentially preserved even after long time cycling. These results further illustrate the architectural merit of the as-

prepared nano NVP@C with high electrochemical performance.

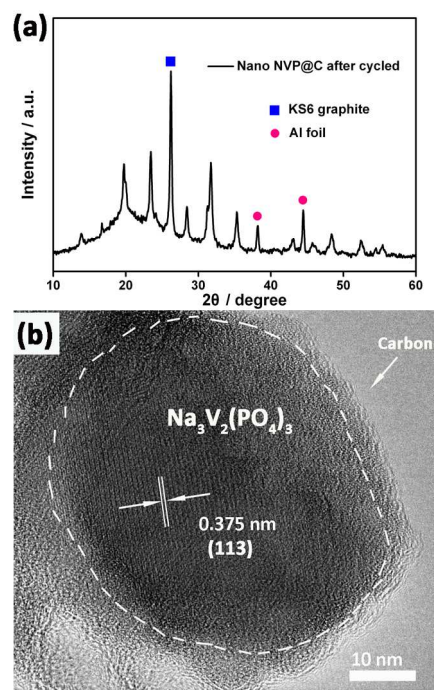
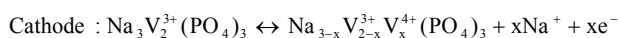
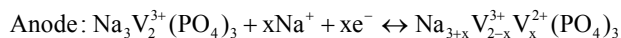


Fig. 6 (a) XRD pattern and (b) HRTEM image of nano NVP@C electrode after cycling for 50 cycles at 1C rate.

The as-prepared nano NVP@C can also be used as anode material for sodium ion batteries. Cyclic voltammogram profiles were recorded for nano NVP@C half cell in the range of 1.3 to 3.8 V (Fig. S7). Two obviously sharp redox peaks were observed in the low voltage and high voltage regions, which correspond to the anode reaction and cathode reaction, respectively. Hence, the anode performance of nano NVP@C was evaluated. The typical charge and discharge profiles at 0.2C in voltage range of 1.3–2 V are displayed in Fig. 7a. The voltage plateaus located around 1.64 V corresponds to the  $\text{V}^{3+}/\text{V}^{2+}$  redox couple, agreeing well with previous studies.<sup>18</sup> By combining the carbon coating and nanosizing, nano NVP@C also exhibited favorable cycle performance (Fig. 7b), displaying an initial charge capacity of  $70.7 \text{ mAh g}^{-1}$  with a capacity retention of 93.2% after 50 cycles. This is comparable with previously results.<sup>15,18,35</sup>

Motivated by the above results, a full cell based on the nano NVP@C as both cathode and anode was built. Similar to the  $\text{Li}_3\text{V}_2(\text{PO}_4)_3$  system,<sup>41</sup> the cell reactions in the full cells of  $\text{Na}_3\text{V}_2(\text{PO}_4)_3$  are described as follows:



## ARTICLE

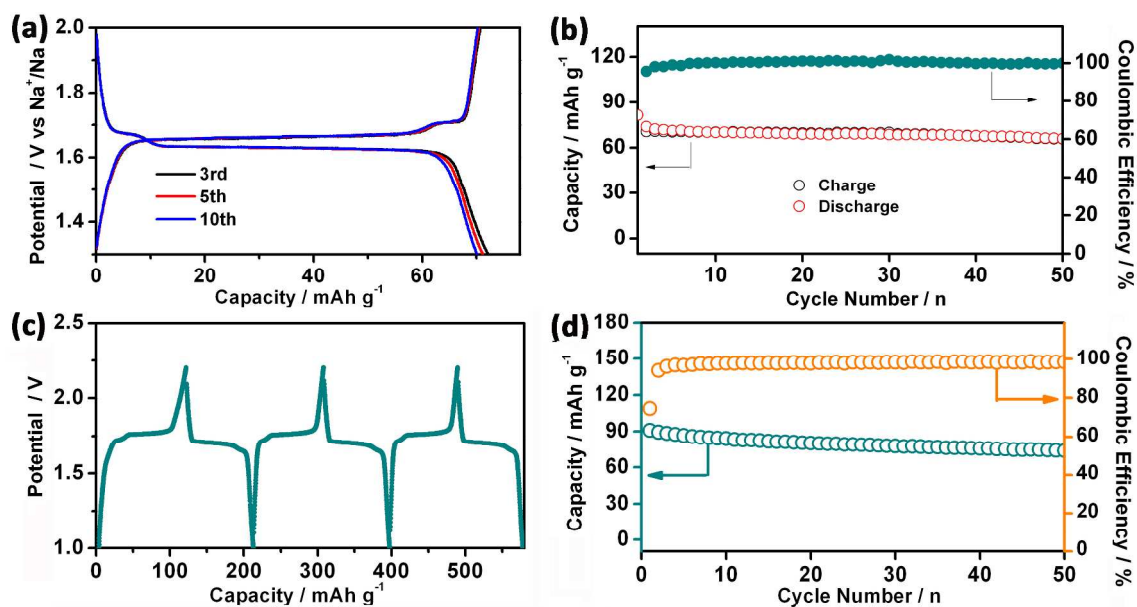


**Fig. 7** (a) Voltage profiles and (b) capacity retention of nano NVP@C at 0.2C rate in the voltage range of 1.3–2.0V; (c) 2C charge/discharge profiles and (d) cycling performance of the full cell employing nano NVP@C as both the cathode and anode in the voltage range of 1–2.2V.

As anticipated, these full cells exhibited open-circuit voltage near zero, as the initial active materials of both electrodes are the same. During the charge/discharge process, the cathode and anode material undergo the reversible electrochemical reactions of  $\text{Na}_3\text{V}_2(\text{PO}_4)_3/\text{NaV}_2(\text{PO}_4)_3$  and  $\text{Na}_3\text{V}_2(\text{PO}_4)_3/\text{Na}_5\text{V}_2(\text{PO}_4)_3$ , respectively. Fig. 7c illustrates the typical charge-discharge curves of the full cell cycled between 1–2.2V. Two distinct voltage plateaus during the charge process and one during the discharge process were observed. This feature is in accordance with the CV profile (Fig. S8). The full cell utilizes the existing concept but offers better performance than that of prior system.<sup>41</sup> It delivered a reversible capacity of  $90.9 \text{ mAh g}^{-1}$  at 2C with an output voltage of about 1.7V, corresponding to a specific energy density of about  $154.5 \text{ Wh kg}^{-1}$ . Furthermore, the capacity retention reached 81.4% after 50 cycles (Fig. 7d). With a cathode limited design, the estimated capacity is based on the active mass of cathode material. Additionally, the Coulombic efficiency is increased to about 99% within 5 cycles and then maintains for the measured 50 cycles, which shows the feasibility for practical applications.

Based on the above results, nano NVP@C indeed has better electrochemical properties than that of the other two samples. The advantages of nano NVP@C core-shell structure are easily accountable. As illustrated in Fig. 8, for NVP (Fig. 8a), as a result of the limited diffusion length, the reaction of  $\text{Na}^+$  can only occur on the outside part of the big particles. Meanwhile, the transfer of  $\text{e}^-$  is blocked by the

hampered conductivity, leading to poor performance. For NVP/C (Fig. 8b), the conductivity is increased in a way, but part of the big particles is still kept inactive due to the long ion diffusion passage. However, for nano NVP@C (Fig. 8c), the core-shell structure with small particle size and conductive carbon coating offers sufficient electric and ionic conduction. This enables the full utilization of the active material with high capacity, long cyclability and high rate capability.

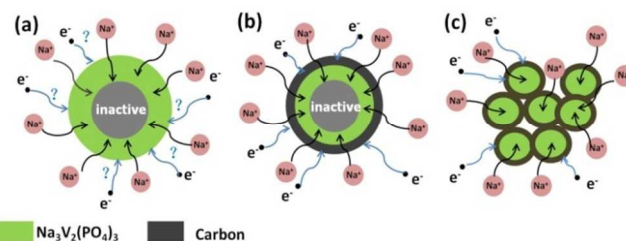


**Fig. 8** Schematic illustration of electron conduction and  $\text{Na}^+$  transport within (a) NVP, (b) NVP/C, and (c) nano NVP@C.

## 45 Conclusions

In summary, a nano core-shell  $\text{Na}_3\text{V}_2(\text{PO}_4)_3@\text{C}$  material with particle size of around 40 nm has been successfully prepared using a hydrothermal assisted sol-gel method. The as-prepared  $\text{Na}_3\text{V}_2(\text{PO}_4)_3@\text{C}$  nanocomposite exhibited

impressive electrochemical performance as cathode materials for NIBs when charged and discharged at the voltage range of 2.5–3.8 V, rendering an initial discharge capacity of 104.3 mAh g<sup>-1</sup> at 0.5C and 94.9 mAh.g<sup>-1</sup> at 5C with 96% capacity retention after 700 cycles. Furthermore, the discharge capacities changed slightly when cycled at different rates. Remarkably, a full cell with the as-prepared composite as active material of both positive and negative electrodes offers an output voltage of 1.7 V, a specific capacity of 90.9 mAh g<sup>-1</sup> and a specific energy density of about 154.5 Wh kg<sup>-1</sup>. The synthetic strategy should be helpful for the design of other uniformly nanosized core-shell materials for electrodes with a high-rate requirement.

## Acknowledgements

This work was supported by the Programs of National 973 (2011CB935900), NSFC (21231005 and 21322101) and MOE (113016A and B12015).

## Notes and references

Key Laboratory of Advanced Energy Materials Chemistry (Ministry of Education), College of Chemistry, Collaborative Innovation Center of Chemical Science and Engineering, Nankai University, Tianjin 300071, P. R. China. Fax: +86-22-23509571; Tel: +86-22-23506808;

E-mail: chenabc@nankai.edu.cn

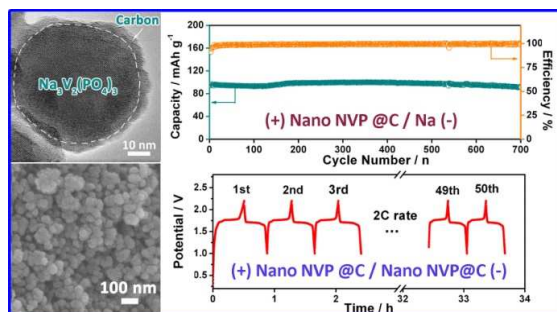
† Electronic Supplementary Information (ESI) available: details of additional pore size distribution curves, XRD patterns, SEM images, nitrogen adsorption and desorption isotherm and cyclic voltammograms. See DOI: 10.1039/b000000x/

1. M. Armand and J. M. Tarascon, *Nature*, 2008, **451**, 652-657.
2. J. B. Goodenough and Y. Kim, *Chem. Mater.*, 2010, **22**, 587-603.
3. F. Y. Cheng, J. Liang, Z. L. Tao and J. Chen, *Adv. Mater.*, 2011, **23**, 1695-1715.
4. B. Dunn, H. Kamath and J. M. Tarascon, *Science*, 2011, **334**, 928-935.
5. M. D. Slater, D. Kim, E. Lee and C. S. Johnson, *Adv. Funct. Mater.*, 2013, **23**, 947-958.
6. V. Palomares, P. Serras, I. Villaluenga, K. B. Hueso, J. Carretero-González and T. Rojo, *Energy Environ. Sci.*, 2012, **5**, 5884-5901.
7. N. Yabuuchi, M. Kajiyama, J. Iwatate, H. Nishikawa, S. Hitomi, R. Okuyama, R. Usui, Y. Yamada and S. Komaba, *Nat. Mater.*, 2012, **11**, 512-517.
8. S. Wang, L. Wang, Z. Zhu, Z. Hu, Q. Zhao and J. Chen, *Angew. Chem. Int. Ed.*, 2014, DOI: 10.1002/anie.201400032.
9. H. Pan, Y. S. Hu and L. Chen, *Energy Environ. Sci.*, 2013, **6**, 2338-2360.
10. S. Y. Hong, Y. Kim, Y. Park, A. Choi, N. S. Choi and K. T. Lee, *Energy Environ. Sci.*, 2013, **6**, 2067-2081.
11. R. Berthelot, D. Carlier and C. Delmas, *Nat. Mater.*, 2011, **10**, 74-80.
12. M. Casas-Cabanas, V. V. Roddatis, D. Saurel, P. Kubiak, J. Carretero-González, V. Palomares, P. Serras and T. Rojo, *J. Mater. Chem.*, 2012, **22**, 17421-17423.
13. M. Avdeev, Z. Mohamed, C. D. Ling, J. Lu, M. Tamaru, A. Yamada and P. Barpanda, *Inorg. Chem.*, 2013, **52**, 8685-8693.
14. P. Senguttuvan, G. Rousse, M. E. Arroyo y de Dompablo, H. Vezin, J. M. Tarascon and M. R. Palacin, *J. Am. Chem. Soc.*, 2013, **135**, 3897-3903.
15. K. Saravanan, C. W. Mason, A. Rudola, K. H. Wong and P. Balaya, *Adv. Energy Mater.*, 2013, **3**, 444-450.
16. Y. H. Jung, C. H. Lim and D. K. Kim, *J. Mater. Chem. A*, 2013, **1**, 11350-11354.
17. H. He, G. Jin, H. Wang, X. Huang, Z. Chen, D. Sun and Y. Tang, *J. Mater. Chem. A*, 2014, **2**, 3563-3570.
18. Z. L. Jian, L. Zhao, H. L. Pan, Y. S. Hu, H. Li, W. Chen and L. Q. Chen, *Electrochem. Commun.*, 2012, **14**, 86-89.
19. Z. L. Jian, W. Z. Han, X. Lu, H. X. Yang, Y. S. Hu, J. Zhou, Z. B. Zhou, J. Q. Li, W. Chen, D. F. Chen and L. Q. Chen, *Adv. Energy Mater.*, 2013, **3**, 156-160.
20. S. Y. Lim, H. Kim, R. A. Shakoor, Y. Jung and J. W. Choi, *J. Electrochem. Soc.*, 2012, **159**, A1393-A1397.
21. Z. L. Gong and Y. Yang, *Energy Environ. Sci.*, 2011, **4**, 3223-3242.
22. L. Wang, K. Zhang, Z. Hu, W. Duan, F. Cheng and J. Chen, *Nano Research*, 2013, **7**, 199-208.
23. Z. Hu, K. Zhang, H. Y. Gao, W. C. Duan, F. Y. Cheng, J. Liang and J. Chen, *J. Mater. Chem. A*, 2013, **1**, 12650-12656.
24. W. C. Duan, Z. Hu, K. Zhang, F. Y. Cheng, Z. L. Tao and J. Chen, *Nanoscale*, 2013, **5**, 6485-6490.
25. B. H. Toby, *J. Appl. Crystallogr.*, 2001, **34**, 210-213.
26. J. Gaubicher, C. Wurm, G. Goward, C. Masquelier and L. Nazar, *Chem. Mater.*, 2000, **12**, 3240-3242.
27. W. Song, X. Ji, Z. Wu, Y. Zhu, Y. Yang, J. Chen, M. Jing, F. Li and C. E. Banks, *J. Mater. Chem. A*, 2014, DOI: 10.1039/c4ta00230j3.
28. Z. Z. Zheng, Y. Wang, A. Zhang, T. R. Zhang, F. Y. Cheng, Z. L. Tao and J. Chen, *J. Power Sources*, 2012, **198**, 229-235.
29. M. M. Doeff, Y. Hu, F. McLarnon and R. Kostecki, *Electrochem. Solid-State Lett.*, 2003, **6**, A207-A209.
30. J. D. Wilcox, M. M. Doeff, M. Marcinek and R. Kostecki, *J. Electrochem. Soc.*, 2007, **154**, A389-A395.
31. Z. Zhu, F. Cheng and J. Chen, *J. Mater. Chem. A*, 2013, **1**, 9484-9490.
32. L. L. Li, Y. Cheah, Y. Ko, P. Teh, G. Wee, C. Wong, S. J. Peng and M. Srinivasan, *J. Mater. Chem. A*, 2013, **1**, 10935-10941.
33. X. L. Wu, L. Y. Jiang, F. F. Cao, Y. G. Guo and L. J. Wan, *Adv. Mater.*, 2009, **21**, 2710-2714.
34. C. Sun, S. Rajasekhara, J. B. Goodenough and F. Zhou, *J. Am. Chem. Soc.*, 2011, **133**, 2132-2135.
35. J. Kang, S. Baek, V. Mathew, J. Gim, J. Song, H. Park, E. Chae, A. K. Rai and J. Kim, *J. Mater. Chem.*, 2012, **22**, 20857-20860.
36. R. Dominko, M. Bele, M. Gaberscek, M. Remskar, D. Hanzel, J. M. Goupil, S. Pejovnik and J. Jamnik, *J. Power Sources*, 2006, **153**, 274-280.
37. S. Y. Chung, J. T. Bloking and Y. M. Chiang, *Nat. Mater.*, 2002, **1**, 123-128.
38. H. Gao, Z. Hu, K. Zhang, F. Cheng and J. Chen, *Chem. Commun.*, 2013, **49**, 3040-3042.
39. H. Gao, L. Jiao, W. Peng, G. Liu, J. Yang, Q. Zhao, Z. Qi, Y. Si, Y. Wang and H. Yuan, *Electrochim. Acta*, 2011, **56**, 9961-9967.

40. F. Cheng, H. Wang, Z. Zhu, Y. Wang, T. Zhang, Z. Tao and J. Chen, *Energy Environ. Sci.*, 2011, **4**, 3668-3675.
41. L. S. Plashnitsa, E. Kobayashi, Y. Noguchi, S. Okada and J. i. Yamaki, *J. Electrochem. Soc.*, 2010, **157**, A536-A543.



Table of contents



Na<sub>3</sub>V<sub>2</sub>(PO<sub>4</sub>)<sub>3</sub>@C core-shell nanocomposites were synthesized and applied as electrodes materials in rechargeable sodium batteries, showing remarkable rate capability and cyclability.